Front. Earth Sci. 2019, 13(1): 75–91
https://doi.org/10.1007/s11707-018-0712-1

RESEARCH ARTICLE

Effects of nano-pore system characteristics on CH_4 adsorption capacity in anthracite

Chang'an SHAN (✉)[1,2,3], Tingshan ZHANG[4], Xing LIANG[5], Dongchu SHU[5], Zhao ZHANG[5], Xiangfeng WEI[6], Kun ZHANG[7], Xuliang FENG[1], Haihua ZHU[4], Shengtao WANG[8], Yue CHEN[8]

1 School of Earth Sciences and Engineering, Xi'an Shiyou University, Xi'an 710065, China
2 Shandong Provincial Key Laboratory of Depositional Mineralization & Sedimentary Minerals, Shandong University of Science and Technology, Qingdao 266590, China
3 Key Laboratory of Tectonics and Petroleum Resources (China University of Geosciences), Ministry of Education, Wuhan 430074, China
4 School of Geoscience and Technology, Southwest Petroleum University, Chengdu 610500, China
5 Exploration and Development Department, Zhejiang Oilfield Company, CNPC, Hangzhou 310023, China
6 SINOPEC Exploration Company, Chengdu 610014, China
7 State Key Laboratory of Petroleum Resources and Prospecting, China University of Petroleum, Beijing 102249, China
8 Shaanxi Yanchang Petroleum International Exploration and Development Engineering Co. Ltd, Xi'an 710075, China

Abstract This study aims to determine the effects of nanoscale pores system characteristics on CH_4 adsorption capacity in anthracite. A total of 24 coal samples from the southern Sichuan Basin, China, were examined systemically using coal maceral analysis, vitrinite reflectance tests, proximate analysis, ultimate analysis, low-temperature N_2 adsorption–desorption experiments, nuclear magnetic resonance (NMR) analysis, and CH_4 isotherm adsorption experiments. Results show that nano-pores are divided into four types on the basis of pore size ranges: super micropores (<4 nm), micropores (4–10 nm), mesopores (10–100 nm), and macropores (>100 nm). Super micropores, micropores, and mesopores make up the bulk of coal porosity, providing extremely large adsorption space with large internal surface area. This leads us to the conclusion that the threshold of pore diameter between adsorption pores and seepage pores is 100 nm. The "ink bottle" pores have the largest CH_4 adsorption capacity, followed by semi-opened pores, whereas opened pores have the smallest CH_4 adsorption capacity which indicates that anthracite pores with more irregular shapes possess higher CH_4 adsorption capacity. CH_4 adsorption capacity increased with the increase in NMR porosity and the bound water saturation. Moreover, CH_4 adsorption capacity is positively correlated with NMR permeability when NMR permeability is less than 8×10^{-3} md. By contrast, the two factors are negatively correlated when NMR permeability is greater than 8×10^{-3} md.

Received September 24, 2017; accepted April 10, 2018

E-mail: shanca@xsyu.edu.cn

Keywords CH_4 adsorption capacity, anthracite, nano-pore structure, NMR physical properties

1 Introduction

Coalbeds are self-sourcing reservoirs with different characteristics compared with conventional reservoirs (Ayers, 2002). Coal is a complex heterogeneous mixture of organic (maceral) and inorganic (mineral) components and has a very complicated pore structure (Gürdal and Yalçın, 2001). The types of pores and the formation mechanism of coal molecular structure have been studied by many researchers (Gan et al., 1972; Hao, 1987; Giffin et al., 2013; Pan et al., 2015a, 2017). In almost all coal reservoirs, the pore size distribution ranges from microscopic to macroscopic. Sing (1982) classifies the pores into three categories in the context of physisorption: macropores (>50 nm), mesopores (2−50 nm), and micropores (<2 nm). The pore structure gives coal a strong ability to adsorb gas because it has large internal surface area which provides numerous active sites for CH_4 adsorption (Cai et al., 2013; Pan et al., 2015a). Gray (1987) proposed that approximately 95% of total CH_4 may be adsorbed in the coal matrix. The quantitative evaluation of pore size distribution, pore volume, and pore surface area are very important in understanding CH_4 adsorption capacity and evaluating the gas reserves of coal (Cai et al., 2013; Pan et al., 2015a). The effects of pore structure on CH_4 adsorption capacity has been studied in four bituminous and subbituminous coals from Northeast China (Cai et al.,

2013). The results showed that micropores (2–10 nm) and mesopores (10–100 nm) occur as a part of the coal matrix, providing extremely large internal surface area with a strong affinity to CH_4. Macropores (100–1000 nm) and super macropores (> 1000 nm) likely serve mainly as CH_4 transport pathways, and only a small amount of CH_4 is adsorbed in the surface of these pores (Cai et al., 2013).

The characteristics of coal pores have been studied using numerous experimental test methods, such as gas (N_2 or CO_2) adsorption–desorption analyses (Radovic et al., 1997; Yao et al., 2006; Pan et al., 2015b), nuclear magnetic resonance (NMR) analysis (Yao and Liu, 2006), small angle X-ray scattering (SAXS) (Mitropoulos et al., 1998; Nakagawa et al., 2000; Sastry et al., 2000; Pan et al., 2016), high resolution transmission electron microscopy, quantitative X-ray CT imaging (Karacan and Okandan, 2001), and small-angle neutron scattering (Radlinski et al., 2004). Among these methods, the N_2 adsorption–desorption experiment has been regarded as the most effective method in studying nano-pore structure (Faulon et al., 1994; Diduszko et al., 2000; Fu et al., 2000; Mahnke and Mögel, 2003; Mahamud et al., 2004; Rigby, 2005; Cuerda-Correa et al., 2006). Thus, in this paper, we will study the influence of nano-pore structure by the N_2 adsorption-desorption method in combination with nuclear magnetic resonance (NMR) and CH_4 isotherm adsorption experiments on CH_4 adsorption capacity of samples of Lopingian coal to enhance our understanding of gas storage mechanisms.

2 Samples and methods

2.1 Coal samples

For this study, 24 coal core samples from the Lopingian [Wuchiapingian to Changhsingian (Late Permian), 260–252 Ma] (ICS, 2017) were collected from 11 wells in the coalbed methane (CBM) exploration and production demonstration area in the southern Sichuan basin, China (Fig. 1). To keep samples fresh for extended period of time, all samples were carefully and rapidly covered using cling wrap, and then immediately brought to the laboratory for experiments. The key properties of those coal samples are shown in Table 1. Results of organic petrographic analyses of these samples suggest that the Lopingian coals are typical anthracites with high thermal maturity (the maximum vitrinite reflectance is 2.64%–3.31%). Vitrinite group macerals are the most abundant maceral group, followed by inertinite and inorganic mineral matter.

2.2 Experimental methods

To study the influences of coal nano-pore system characteristics on CH_4 adsorption capacity, 24 samples were examined using coal maceral analysis, vitrinite reflectance tests, proximate analysis, ultimate analysis, low-temperature N_2 adsorption- desorption experiments, NMR analysis, and CH_4 isothermal adsorption experiments.

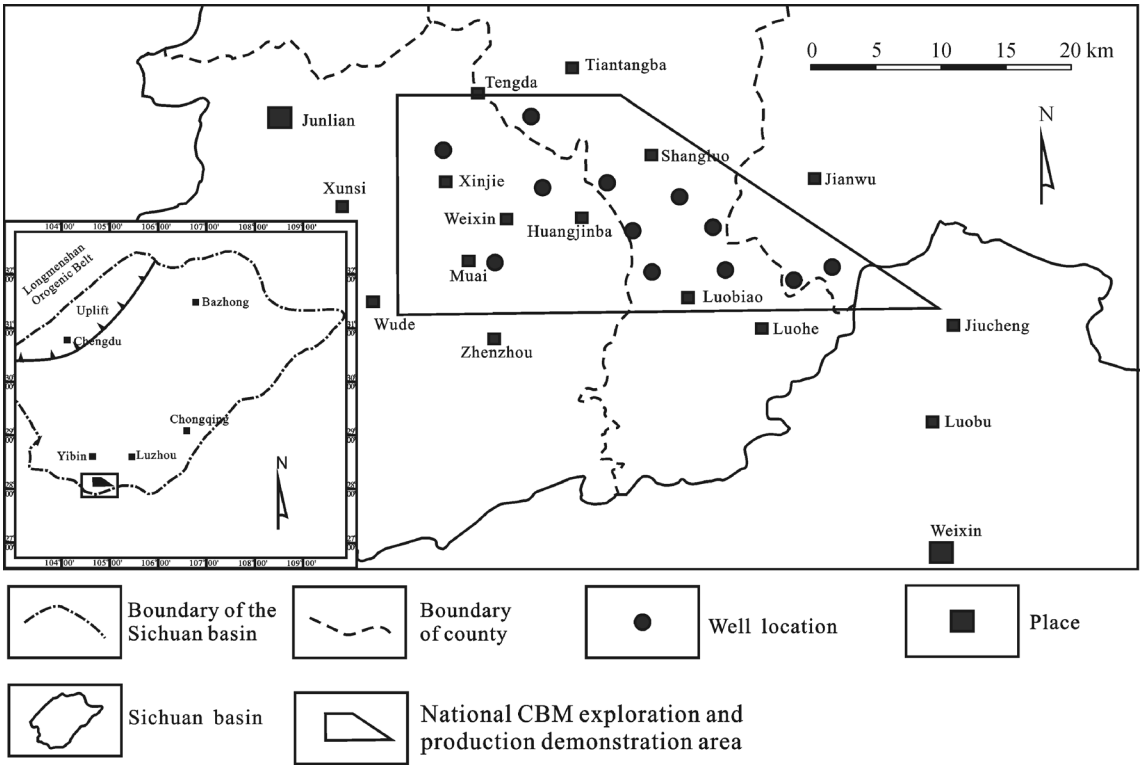

Fig. 1 General tectonic setting, study area location, and study well distribution.

Table 1 Complete list and properties of 24 coal core samples

Sample	Vitrinite/vol.% [a]	Inertinite/vol.% [a]	MM[b]/vol.% [a]	Ro, max/%	Proximate analysis/wt.% [c], ad [d]				Ultimate analysis/wt.% [c], ad [d]		
					M_{ad}[e]	A_{ad}[e]	V_{ad}[g]	FC_{ad}[h]	Carbon	Hydrogen	Nitrogen
L1	92.7	5.3	2	3.12	0.84	31.05	10.1	58.02	57.75	1.77	0.61
L2	65	33.5	1.5	3.13	0.72	26.13	10.83	62.33	63.98	2.09	0.62
L3	18.4	69.6	12	3.31	0.75	21.21	8.01	70.04	67.81	2.38	0.71
L4	70.1	24.1	5.8	2.91	0.47	34.58	13.41	51.54	53.84	1.63	0.38
L5	44.8	51.2	4	3.09	0.55	29.9	7.97	61.58	61.52	2.03	0.55
L6	84.8	8.5	6.7	3.05	0.78	30.11	9.28	59.83	60.69	2.07	0.59
L7	22.9	75.7	1.4	3.01	0.75	19.3	7.7	72.26	71.7	2.56	0.86
L8	68.9	30.1	1	2.92	1.1	14.72	8.88	75.31	75.72	2.67	0.82
L9	20.4	78.8	0.8	2.89	0.58	33.12	6.9	59.41	60.3	1.91	0.49
L10	67.9	14.3	17.8	2.85	0.83	32.98	8.29	57.91	57.32	1.95	0.59
L11	81.2	6.5	12.3	2.94	0.72	29.11	8.65	61.53	62.28	2.05	0.56
L12	90	8.7	1.3	3.12	0.79	20.2	9.05	69.97	71.59	2.34	0.76
L13	87.8	7	5.2	3.09	0.83	19.53	8.33	71.32	71.39	2.38	0.84
L14	56.6	39.7	3.7	3.18	0.93	26.12	7.97	64.99	64.21	2.23	0.75
L15	73.5	20.5	6	3.29	0.69	24.36	11.17	63.79	65.06	2.05	0.61
L16	84.5	5.8	9.7	2.73	0.77	23	9.16	67.07	67.65	2.47	0.7
L17	65.7	29.7	4.6	2.64	0.69	28.38	9.17	61.76	62.53	2.29	0.74
L18	79.2	19.5	1.3	2.84	0.83	10.6	7.31	81.27	80.39	3.08	1.15
L19	60.5	38	1.5	2.87	0.58	31.82	8.71	58.9	59.83	2.15	0.62
L20	21	78	1	2.96	0.59	18.7	8.19	72.53	72.15	2.75	0.92
L21	87.6	7.8	4.6	3.16	0.48	43.5	7.06	48.96	48.88	1.46	0.4
L22	45.7	51	3.3	3.26	0.59	29.25	11.44	58.73	60.94	1.74	0.53
L23	25.1	71.9	3	3.09	0.73	37.74	7.91	53.64	51.09	1.61	0.56
L24	82.2	11.8	6	3.11	0.67	34.81	9.81	54.71	53.01	1.43	0.48

a) vol.%: volume percent; b) MM: mineral matter; c) wt.%: mass percent; d) ad: as received basis; e) M_{ad}: moisture content; f) A_{ad}: ash yield; g) V_{ad}: volatile content; h) FC_{ad}: fixed carbon content.

2.2.1 Vitrinite reflectance and maceral composition analysis

Mean maximum vitrinite reflectance (% Ro, max) measurements and maceral group analysis (500 points) were performed in accordance with China National Standards GB/T 6948-2008 and GB/T 5588-2001, respectively. The procedures were conducted on the same polished section of the coal samples using a Leitz MPV-3 photometer microscope.

2.2.2 Proximate and ultimate analyses

Proximate analysis (following China National standards GB/T 212-2008) was performed on the 24 coal core samples. The analysis was conducted on a fully auto-measuring industrial analyzer to determine ash yield, moisture content, volatile material yield, and fixed carbon contents under air dry basis. Ultimate analysis was conducted according to China National standards GB/T 476-2001 using an element analyzer to measure carbon, hydrogen, and nitrogen elements of the 24 samples.

2.2.3 Low-temperature N_2 adsorption–desorption experiment

Low-temperature N_2 adsorption–desorption isotherms were obtained using a Quantachrome QUADRASORB SI Surface Area and Pore Size Analyzer at 77 K following the Chinese petroleum industry standard specification SY/T 6154-1995. Coal samples were crushed into grains of 60–80 mesh size (180–250 μm), dried in an oven at 383 K for 24 h, and degassed under high-vacuum apparatus (< 10 mmHg) for 12 h at 383 K. The saturation vapor pressure (p_o) of N_2 at 77 K was determined every 2 h during the experiment using a nitrogen vapor pressure thermometer. The relative pressure (p/p_o) ranged from 0.011 to 0.995, and both adsorption–desorption isotherms were measured to investigate the hysteresis types.

2.2.4 NMR experiment

NMR is used to test movable fluid volume in pores to reflect the effective porosity of the core samples; subsequently, the porosity and irreducible water saturation are utilized to calculate the permeability of the core samples. In the present study, 24 core samples were analyzed using an NMR core analyzer with low magnetic field (RecCore04), in accordance with the Chinese petroleum industry standard specification SY/T6490-2007. In the magnetic field, the NMR signals of a hydrogen nucleus (^{1}H) present within the pore fluid of a rock can be detected through a relationship between relaxation distribution and relaxation time. This produces the T_2 spectrum. The parameter "T_2" is used to characterize the NMR signal, that is (Kenyon, 1992):

$$T_2 = \frac{V}{\rho S}, \tag{1}$$

where T_2 represents the relaxation time of the fluid in the rock, ρ is a constant that represents the relaxation intensity of the rock surface, S represents the surface area of the pores, and V represents the volume of the pores.

Thus, physical properties such as porosity, rock permeability, and flow characteristics (including bound water saturation and movable water saturation of the pore fluids) can be determined by the T_2 relaxation time (Coates et al., 1999; Shan et al., 2015). The area greater than the T_2 cutoff value corresponds to the volume of the movable fluid and that area smaller than the T_2 cutoff value represents the volume of the bound fluid. For this purpose, the saturation of the bound water and the movable fluid can be calculated. The porosity of the samples is calculated directly using the following equation (Hodgkins and Howard, 1999):

$$\Phi = \left(\frac{A_t}{V_t}\right) * a + b, \tag{2}$$

where Φ is the NMR porosity, A_t represents the total NMR signal, V_t is the total volume of the sample, and both a and b are calibration coefficients from test signals of all samples with a linear fit.

According to the bound water saturation, the movable water saturation, and NMR porosity, the NMR permeability can be calculated using the Coates model (Coates et al., 1999):

$$K = \left(\frac{\Phi}{C}\right)^4 \times \left(\frac{S_{wm}}{S_{wb}}\right)^2, \tag{3}$$

where K is the NMR permeability, Φ is the NMR porosity, S_{wm} represents the movable water saturation, S_{wb} is the bound water saturation, and C is the undetermined permeability coefficient.

2.2.5 CH_4 isotherm adsorption experiment

CH_4 isotherm adsorption experiments were measured using the TerraTek Isotherm Measurement System (IS–100) according to the previous research (Yao et al., 2008). All coal samples were prepared for moisture-equilibrium treatment by crushing and sieving to a size range of 0.18–0.25 mm (60–80 mesh) with a weight of 100–125 g (American Society for Testing Material standard). Moisture-equilibrium treatment was processed for at least four days for each sample. After these pretreatments, the coal was placed into the sample cell of the IS-100 for the adsorption isotherm test. The temperature and equilibrium pressure were 28°C and 10 MPa, respectively. Analytical results include the Langmuir volume (V_L) and Langmuir pressure (P_L) under three bases (i.e., air dry, dry ash-free, and equilibrium moisture).

3 Results

3.1 Nano-pore structures

The total specific surface areas (S_{BET}) calculated from the Brunauer–Emmet–Teller (BET) equation (Brunauer et al., 1938) of the 24 coal core samples by the N_2 adsorption analyses range from 0.611 m^2/g to 2.233 m^2/g and average to 1.312 m^2/g (Table 2). The total pore volumes (V_{BJH}) from Barrett–Joyner–Halenda (BJH) model (Barrett et al., 1951) of the samples range from 1.751×10^{-3} cm^3/g to 5.249×10^{-3} cm^3/g, with an average of 2.641×10^{-3} cm^3/g (Table 2). The pore diameters of the samples are calculated using the BJH model based on the desorption isothermal. The average pore diameter (d_{BJH}) ranges from 6.135 nm to 17.842 nm (Table 2). The N_2 adsorption amount varies from 1.0679 cm^3/g to 3.3532 cm^3/g, with an average of 1.6528 cm^3/g for all samples (Table 2). N_2 adsorption shows positive relationships with S_{BET} and V_{BJH} (Fig. 2).

A plot of the specific surface area with respect to pore diameter (dS_{BJH}/dW versus W) is given in Fig. 3(a). The plot of dS_{BJH}/dW versus W shows that pores in the size range less than 4 nm make up the main contribution to the pore surface area, and the pore concentration decreases with increasing pore size. Figure 3(b) shows the relationship between pore volume and pore-size distribution (dV_{BJH}/dW versus W), which indicates that pores with a diameter larger than 10 nm give the greater contribution to the pore volume. That is, pores less than 4 nm make up the bulk of coal porosity but pores larger than 10 nm can contribute significantly to the total pore volume. Based on this results and previous studies (Hodot, 1966; Shi and Durucan, 2005; Yao et al., 2008, 2009), nano-pores are divided into super micropores (<4 nm), micropores (4–10 nm), mesopores (10–100 nm), and macropores (>100 nm) in this study.

Table 2 Coal structure analysis results from low-temperature N_2 adsorption- desorption analyses of 24 coal core samples

Sample name	d_{BJH} /(nm)	S_{BET} / ($m^2 \cdot g^{-1}$)	N_2 adsorbed amount/ ($cm^3 \cdot g^{-1}$)	$S_{BJH}/(m^2 \cdot g^{-1})$								$V_{BJH}/(\times 10^{-3}\ cm^3 \cdot g^{-1})$								
				S_{total}	super micropores (<4 nm)		Micropores (4–10 nm)		Mesopores (10–100 nm)		Macropores (>100 nm)		V_{total}	super micropores (<4 nm)		Micropores (4–10 nm)		Mesopores (10–100 nm)		Macropores (>100 nm)	
					$S_{s\text{-}mic}$	Percentage /%	S_{mic}	Percentage /%	S_{mes}	Percentage /%	S_{mac}	Percentage /%		$V_{s\text{-}mic}$	Percentage /%	V_{mic}	Percentage /%	V_{mes}	Percentage /%	V_{mac}	Percentage /%
L1	8.654	2.233	2.8553	2.021	1.026	50.8	0.663	32.8	0.323	16	0.009	0.4	4.364	0.745	17.1	1.068	24.5	2.157	49.4	0.394	9
L2	8.074	2.042	2.3287	1.761	0.988	56.1	0.546	31	0.205	11.6	0.022	1.2	3.554	0.773	21.8	0.876	24.6	1.287	36.2	0.618	17.4
L3	8.38	1.26	1.6346	1.249	0.705	56.4	0.378	30.3	0.16	12.8	0.006	0.5	2.616	0.521	19.9	0.596	22.8	1.188	45.4	0.311	11.9
L4	7.161	1.411	1.3031	1.082	0.599	55.4	0.366	33.8	0.114	10.5	0.003	0.3	1.933	0.462	23.9	0.593	30.7	0.751	38.9	0.127	6.6
L5	11.039	1.268	2.1651	1.229	0.634	51.6	0.344	28	0.234	19	0.017	1.4	3.394	0.474	14	0.57	16.8	1.674	49.3	0.676	19.9
L6	8.258	1.322	1.6838	1.294	0.592	45.7	0.499	38.6	0.191	14.8	0.012	0.9	2.671	0.452	16.9	0.797	29.8	0.995	37.3	0.427	16
L7	7.276	1.104	1.2754	1.125	0.655	58.2	0.345	30.7	0.116	10.3	0.009	0.8	2.048	0.481	23.5	0.551	26.9	0.73	35.6	0.286	14
L8	6.535	1.21	1.3463	1.377	0.813	59	0.449	32.6	0.11	8	0.005	0.4	2.25	0.59	26.2	0.726	32.3	0.67	29.8	0.264	11.7
L9	13.49	1.549	3.3532	1.556	0.671	43.1	0.486	31.2	0.363	23.3	0.036	2.3	5.251	0.487	9.3	0.8	15.2	2.739	52.2	1.225	23.3
L10	8.051	0.918	1.0942	0.87	0.456	52.4	0.308	35.4	0.103	11.8	0.003	0.3	1.751	0.348	19.9	0.472	27	0.808	46.1	0.123	7
L11	6.742	1.06	1.0679	1.053	0.681	64.7	0.28	26.6	0.084	8	0.008	0.7	1.776	0.485	27.3	0.427	24	0.577	32.5	0.287	16.2
L12	6.135	1.788	1.2238	1.417	0.87	61.4	0.431	30.4	0.107	7.5	0.009	0.7	2.173	0.629	28.9	0.659	30.3	0.62	28.5	0.265	12.2
L13	7.829	1.473	1.1884	1.002	0.613	61.2	0.283	28.2	0.1	10	0.006	0.6	1.962	0.451	23	0.434	22.1	0.783	39.9	0.294	15
L14	10.199	1.035	1.6357	0.998	0.471	47.2	0.328	32.9	0.187	18.7	0.012	1.2	2.544	0.365	14.3	0.537	21.1	1.245	48.9	0.397	15.6
L15	17.842	0.611	1.5834	0.551	0.221	40.1	0.163	29.6	0.156	28.3	0.011	2	2.46	0.171	7	0.272	11.1	1.497	60.9	0.52	21.1
L16	8.73	1.564	2.2196	1.629	0.972	59.7	0.452	27.7	0.193	11.8	0.012	0.7	3.555	0.696	19.6	0.701	19.7	1.632	45.9	0.526	14.8
L17	8.68	1.129	1.4761	1.122	0.602	53.7	0.374	33.3	0.139	12.4	0.007	0.6	2.436	0.465	19.1	0.577	23.7	1.052	43.2	0.342	14
L18	8.984	1.281	1.9808	1.439	0.812	56.4	0.434	30.2	0.183	12.7	0.01	0.7	3.231	0.596	18.4	0.68	21	1.494	46.2	0.461	14.3
L19	6.471	1.192	1.1145	1.187	0.699	58.9	0.359	30.2	0.127	10.7	0.002	0.2	1.921	0.515	26.8	0.558	29	0.789	41.1	0.059	3.1
L20	7.236	1.416	1.3255	1.167	0.655	56.1	0.387	33.2	0.118	10.1	0.007	0.6	2.111	0.506	24	0.604	28.6	0.74	35.1	0.262	12.4
L21	6.947	1.536	1.7399	1.65	0.959	58.1	0.517	31.3	0.16	9.7	0.014	0.8	2.866	0.701	24.5	0.812	28.3	0.972	33.9	0.381	13.3
L22	9.045	1.297	1.5318	1.074	0.585	54.5	0.361	33.6	0.12	11.2	0.008	0.8	2.428	0.452	18.6	0.555	22.9	1.032	42.5	0.389	16
L23	9.295	0.797	1.2053	0.839	0.432	51.5	0.288	34.3	0.112	13.4	0.007	0.8	1.949	0.328	16.8	0.44	22.6	0.878	45	0.304	15.5
L24	8.961	0.98	1.3346	0.961	0.533	55.5	0.303	31.5	0.119	12.4	0.006	0.6	2.153	0.407	18.9	0.475	22.1	0.963	44.7	0.308	14.3

S_{BET} = the total specific surface area calculated based on the BET equation; S_{BJH},V_{BJH}, d_{BJH} = the total specific surface area, the total pore volume, the average pore diameter calculated using the BJH model; S_{total} = the total pore specific surface area; V_{total} = the total pore volume; $S_{s\text{-}mic}$,$V_{s\text{-}mic}$ = pore specific surface area, pore volume of pores with a diameter of less than 4 nm; S_{mic}, V_{mic} = pore specific surface area, pore volume of pores with a diameter between 4 nm and 10 nm; S_{mes}, V_{mes} = pore specific surface area, pore volume of pores with a diameter between 10 nm and 100 nm; S_{mac}, V_{mac} = pore specific surface area, pore volume of pores with a diameter larger than 100 nm; Percentage = the average pore specific surface area or pore volume percentage of super micropores, micropores, mesopores, and macropores.

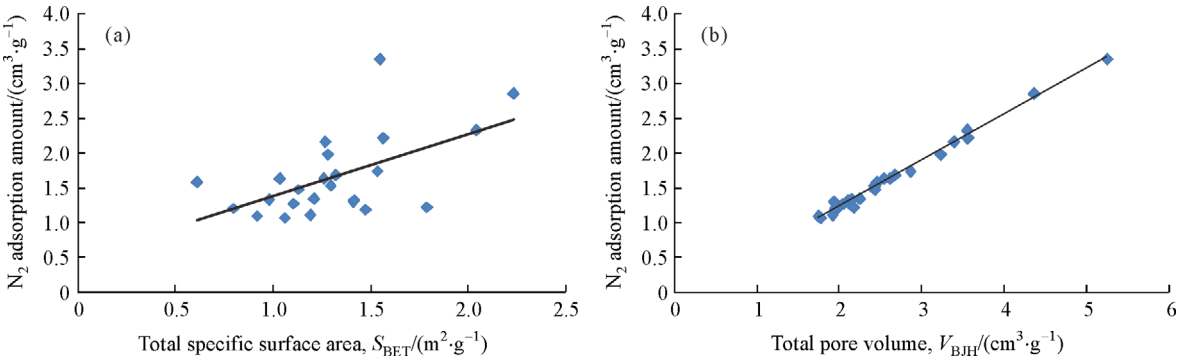

Fig. 2 Relationships between N_2 adsorption amount and S_{BET}, V_{BJH}: (a) relationship between N_2 adsorption amount and S_{BET}; (b) relationship between N_2 adsorption amount and V_{BJH}. S_{BET} = total specific surface area calculated using the BET equation; V_{BJH} = pore volume calculated using the BJH model.

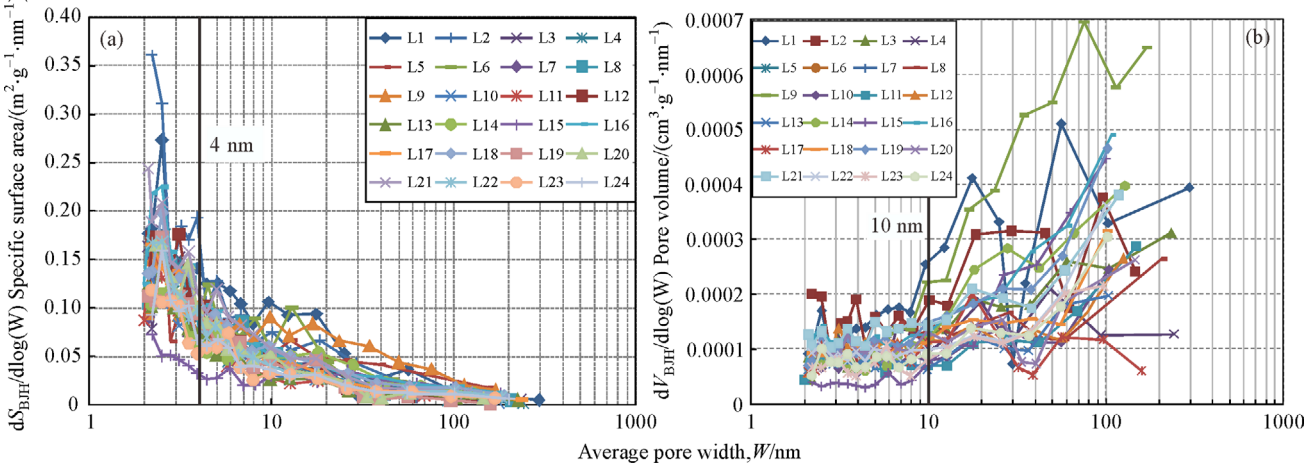

Fig. 3 (a) The relationship between pore-size distribution and the specific surface area; (b) the relationship between pore-size distribution and pore volume. S_{BJH} = the specific surface area calculated using the BJH equation; V_{BJH} = the pore volume calculated using the BJH model.

3.2 Nano-pore shapes

We analyzed 24 coal core samples using the low–temperature N_2 adsorption–desorption experiment. Results show that the N_2 adsorbed amount increases as the pressure increases in all samples. At the pressure range from 0 to approximately 0.9 p/p_o, the adsorption isotherms fit Henry's law very well, but the latter part of the adsorption curves rise more rapidly (Figs. 4(b), 5(b), and 6(b)), like the "Type II" isotherm (Sing, et al., 1982). The increased N_2 adsorption capacity is caused by capillary condensation in the large coal pores. The relationships between low–temperature N_2 adsorption–desorption isotherms (also known as hysteresis loops) can be used to qualitatively predict the shapes of nanoscale coal pores (De Boer, 1958). The shapes of the hysteresis loops have been grouped into three types: Type D1 (Fig. 4(a)), Type D2 (Fig. 5(a)), and Type D3 (Fig. 6(a)).

Coal pores are also divided into three typical types: Type A, Type B, and Type C (Chen and Tang, 2001). Type A comprises opened pores, including cylinder cavities opened at both ends and parallel plane pores opened on all sides (Fig. 5(c)). Type B comprises semi-closed pores, including cylinder cavities, parallel plane pores, wedge-shaped pores, and tapered holes (Figs. 4(c), 5(c), and 6(c)), all of which are closed at one end. Type C is a special pore with narrow neck and wide body and is often referred to as an "ink bottle" pore (Fig. 6(c)).

The hysteresis loops of 8 coal samples of L10, L11, L12, L13, L14, L15, L16, and L22 belong to D1 type (Figs. 4(a) and 4(b)). The adsorption and desorption curves of this type are nearly all overlapped or overlapped in the low relative pressure part and separated in the high relative pressure part. However, the distance between the adsorption branch and the desorption branch is very short in the separated part, which reflects the poor connectivity of Type B pores (Fig. 4(c)). D2 type is represented by 10 samples of L3, L6, L7, L8, L17, L18, L19, L21, L23, and L24

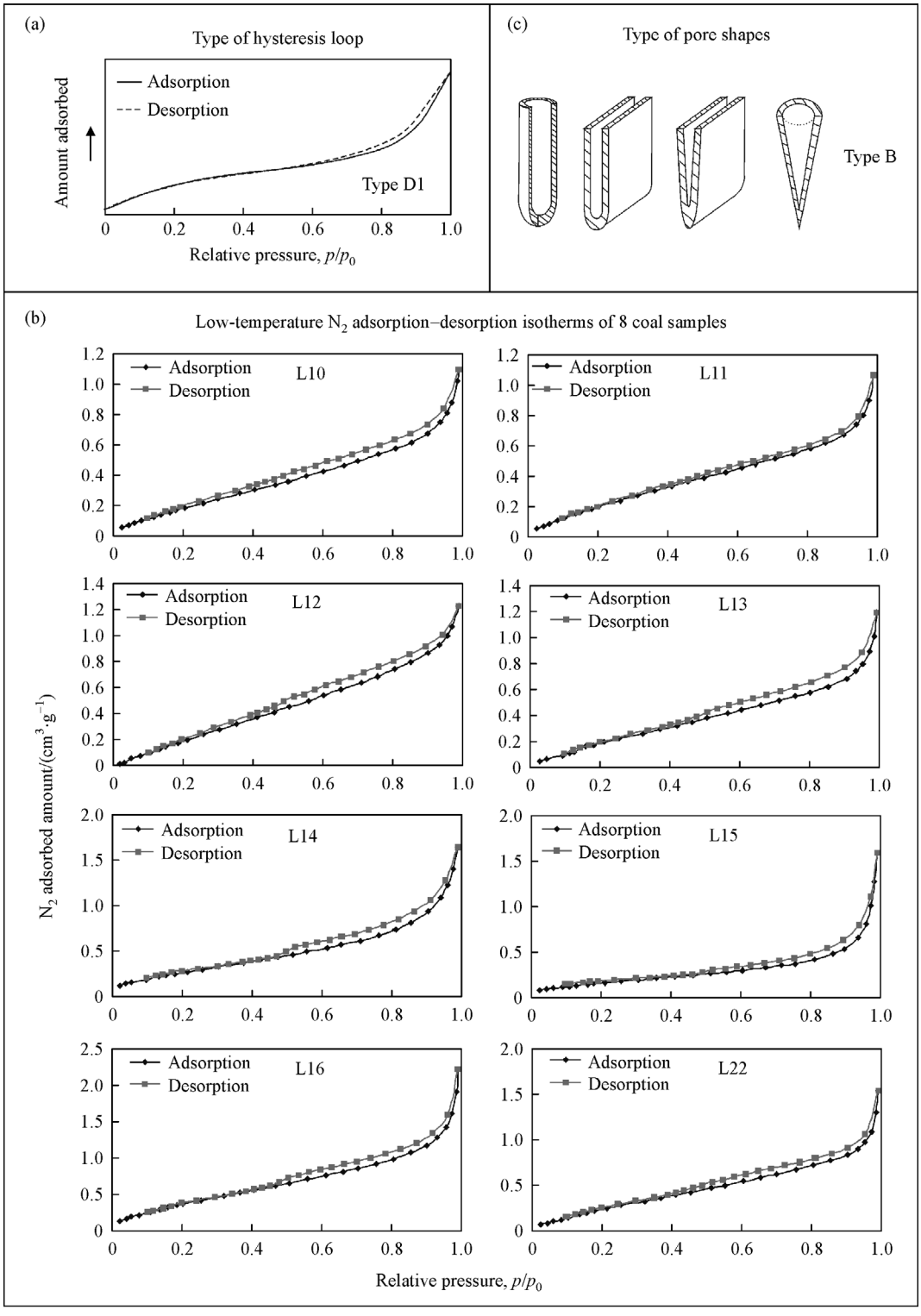

Fig. 4 (a) D1 type of the hysteresis loops; (b) low-temperature N_2 adsorption–desorption isotherms of 8 samples; (c) shapes of nanoscale coal pores.

(Figs. 5(a) and 5(b)). The adsorption and desorption curves are obviously separated in the high relative pressure part, which reflects that coal pores with larger pore size must contain opened pores and may have semi-closed pores. The adsorption branch and desorption branch are overlapped in the low relative pressure part, which reflects that coal pores with smaller pore size are mostly semi-closed pores. That is, these coal pores are composed of Type A

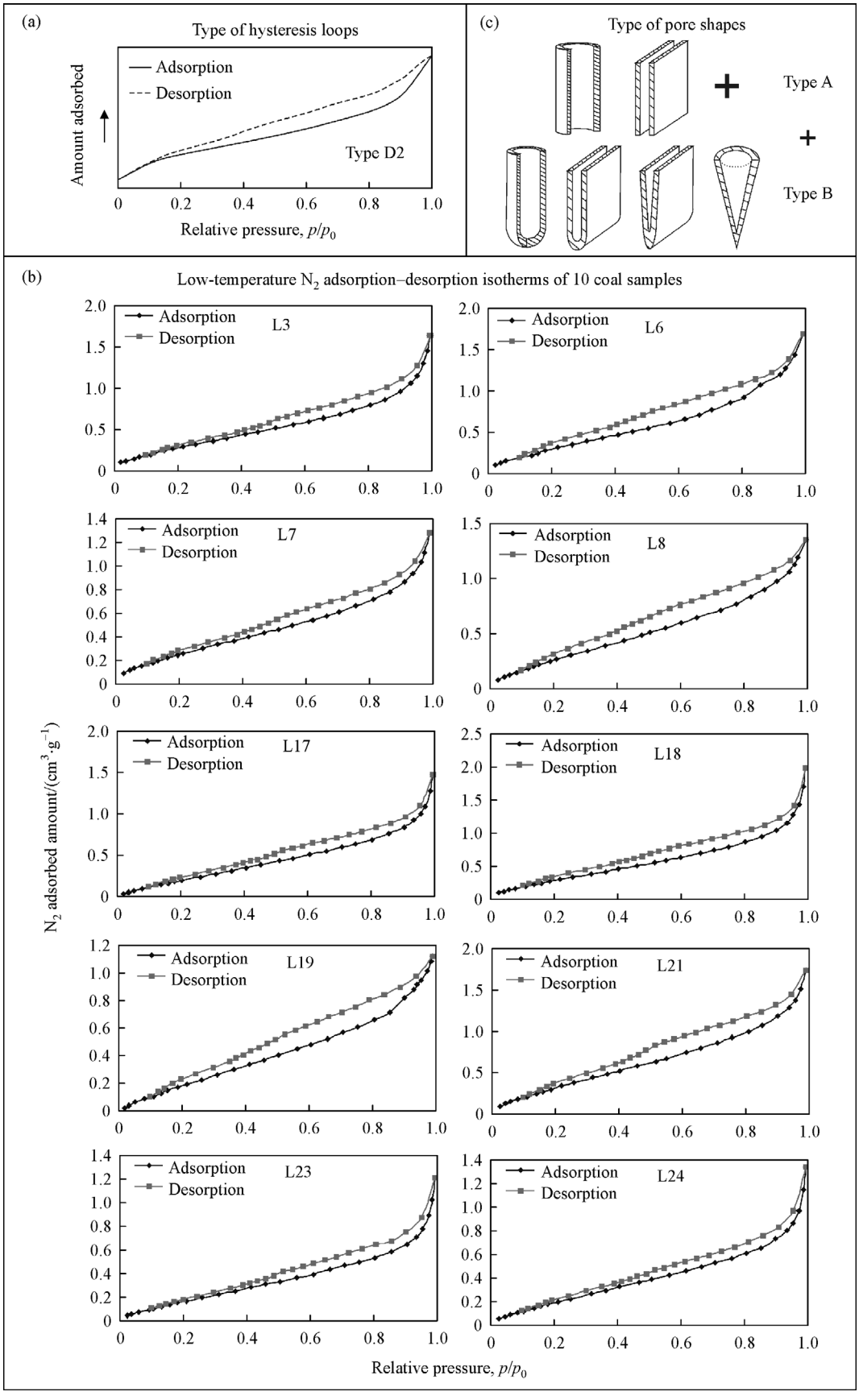

Fig. 5 (a) D2 type of the hysteresis loops; (b) low-temperature N_2 adsorption–desorption isotherms of 10 samples; (c) shapes of nanoscale coal pores.

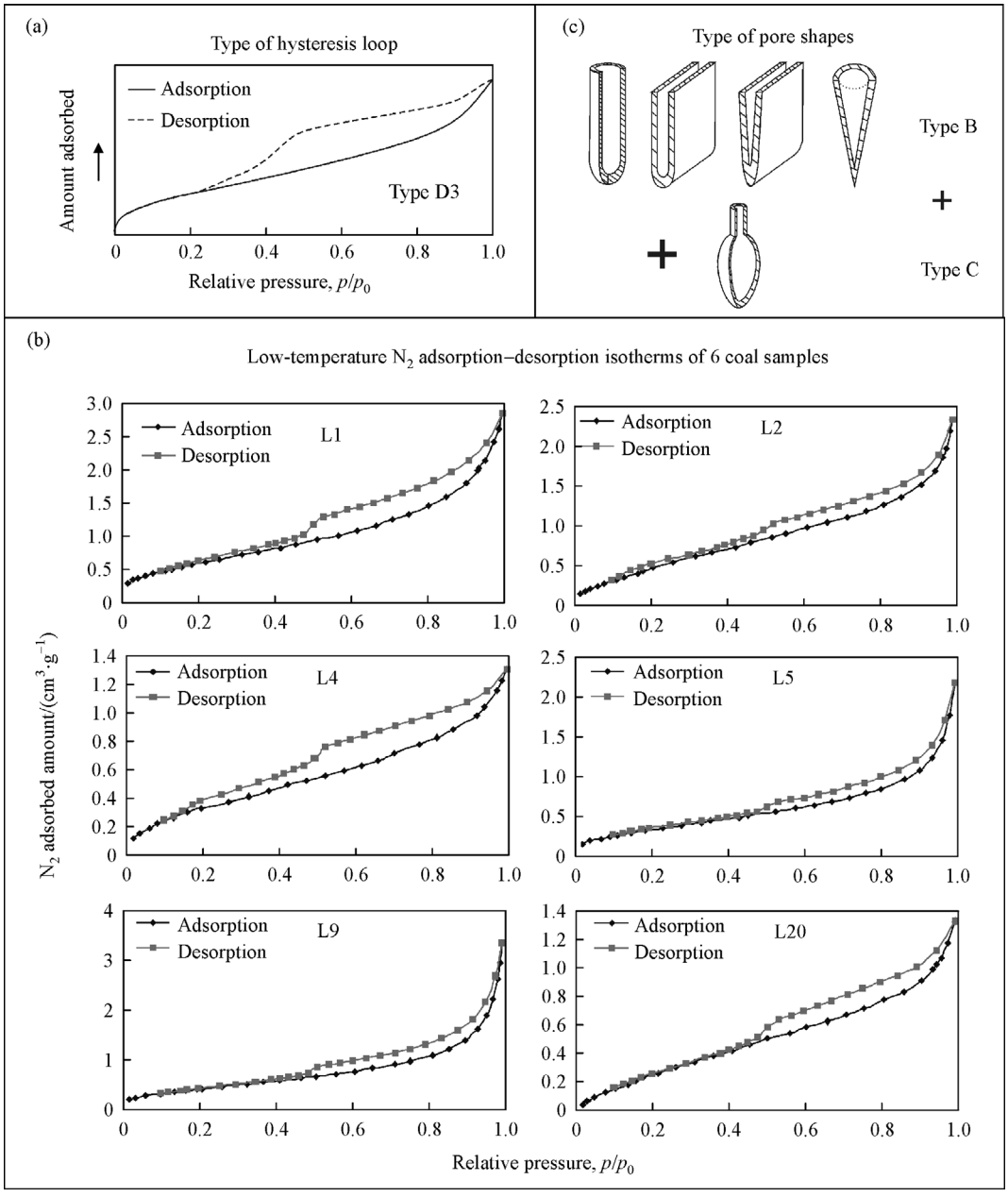

Fig. 6 (a) D3 type of the hysteresis loops; (b) low-temperature N_2 adsorption–desorption isotherms of 6 samples; (c) shapes of nano-pores.

and Type B (Fig. 5(c)). The shape of D3 type is special, the hysteresis loops of 6 coal samples of L1, L2, L4, L5, L9, and L20 are the quintessential example of this type (Figs. 6(a) and 6(b)). The desorption branch shows a hysteresis pattern and a plateau at high p/p_o (>0.5), then falls suddenly to overlap the adsorption branch (<0.5 p/p_o). It shows that pore system consisted of Type B pores and Type C pores (Fig. 6(c)).

3.3 NMR physical properties

24 coal core samples were tested using NMR experiment in this study. The NMR transverse relaxation time (T_2) spectral response characteristics of all samples are shown in Fig. 7. All the experimental data can be seen in Table 3. The porosities of all samples obtained from the NMR tests range from 2.50% to 8.67% and average to 5.13%. The permeability measurements range from 0.0098×10^{-3} md to 20.4739×10^{-3} md with an average of 3.3023×10^{-3} md. The bound water saturations range from 74.12% to 98.09% and average to 87.33%. The movable water saturations range from 1.91% to 25.88% and average to 12.67%.

3.4 Adsorption capacity from CH_4 isotherms

Results from CH_4 isotherm adsorption experiments under

Table 3 Results of 24 coal core samples from nuclear magnetic resonance (NMR) experiments

Sample	Sample volume /cm^3	Calibration coefficient *a*	Calibration coefficient *b*	Permeability coefficient *C*	NMR porosity /%	NMR permeability /($\times10^{-3}$ md)	Bound water saturation /%	Movable water saturation /%	T_2 cutoff value /ms
L1	5.31	0.04595	−0.370168	10	6.7	8.1148	91.74	8.26	33
L2	7.55	0.04595	−0.370168	10	5.58	1.7149	88.26	11.74	33
L3	7.36	0.04595	−0.370168	10	4.08	0.1607	92.93	7.07	33
L4	13.91	0.04595	−0.370168	10	4.49	0.5833	89.29	10.71	33
L5	8.67	0.04595	−0.370168	10	8.67	8.6344	88.99	11.01	33
L6	11.85	0.04595	−0.370168	10	3.72	0.1072	93.03	6.97	33
L7	10.93	0.04595	−0.370168	10	3.57	0.3471	87.24	12.76	33
L8	12.62	0.04595	−0.370168	10	4.17	0.5985	87.66	12.34	33
L9	7.86	0.04595	−0.370168	10	4.65	1.0377	87.02	12.98	33
L10	15.15	0.04595	−0.370168	10	5.7	0.4399	93.94	6.06	33
L11	11.54	0.04595	−0.370168	10	6.02	2.5442	87.77	12.23	33
L12	7.31	0.04595	−0.370168	10	7.28	20.4739	78.76	21.24	33
L13	9.33	0.04595	−0.370168	10	6.29	4.1861	85.95	14.05	33
L14	7.73	0.04595	−0.370168	10	5.41	1.5718	88.06	11.94	33
L15	11.37	0.04595	−0.370168	10	6.76	11.3663	81.07	18.93	33
L16	12.28	0.04595	−0.370168	10	3.17	0.887	77.2	22.8	33
L17	4.62	0.04595	−0.370168	10	2.5	0.279	78.86	21.14	33
L18	5.06	0.04595	−0.370168	10	5.24	9.1846	74.12	25.88	33
L19	5.58	0.04595	−0.370168	10	5.61	2.6269	86.01	13.99	33
L20	6.7	0.04595	−0.370168	10	5.18	2.0754	85.51	14.49	33
L21	7.1	0.04595	−0.370168	10	4.58	0.8206	87.97	12.03	33
L22	12.09	0.04595	−0.370168	10	6.04	1.4583	90.52	9.48	33
L23	15.55	0.04595	−0.370168	10	3.68	0.032	96	4	33
L24	17.41	0.04595	−0.370168	10	4.01	0.0098	98.09	1.91	33

three different bases (air dry basis, dry ash-free basis, and equilibrium moisture basis) of 24 coal samples are shown in Table 4. The Langmuir volume of air dry basis (V_{Lad}) ranges from 21.71 m^3/t to 33.63 m^3/t, with the average of 27.37 m^3/t. The Langmuir volume of dry ash-free basis (V_{Ldaf}) is between 31.42 m^3/t and 47.00 m^3/t, with the average of 38.01 m^3/t. The Langmuir volume of equilibrium moisture basis (V_{Lem}) ranges from 20.73 m^3/t to 32.37 m^3/t, with an average of 25.96 m^3/t. The Langmuir pressure (P_L) values of the three different bases are the same, ranging from 1.79 MPa to 3.13 MPa, with an average of 2.35 MPa. Results demonstrate that anthracite has a larger CH_4 adsorption capacity than subbituminous and bituminous coals (Yao et al., 2008; Cai et al., 2013).

4 Discussion

4.1 Effects of pore surface and volume on CH_4 adsorption capacity

The effects of pore surface and volume on the CH_4 adsorption capacity of 24 anthracite samples are shown in Fig. 8. The Langmuir volume was calculated on a dry ash-free basis. In general, CH_4 adsorption capacity increased with the increase in pore surface (Fig. 8(a)) and volume (Fig. 8(b)). Coals with higher pore surface area and volume have stronger CH_4 adsorption capability because higher internal surface area and volume provide more adsorption sites and space for CH_4, leading to higher adsorption capacity of coals.

4.2 Effects of pore size ranges on CH_4 adsorption capacity

Based on pore size distribution, nano-pores of the studied coals have been divided into 4 types: super micropores (<4 nm), micropores (4–10 nm), mesopores (10–100 nm), and macropores (>100 nm). To better understand the effects of different pore sizes on CH_4 adsorption capacity, we will discuss the contribution of super micropores (<4 nm), micropores (4–10 nm), mesopores (10–100 nm), and macropores (>100 nm) to the total specific surface area and pore volume, because we know that significant positive correlation exists between CH_4 adsorption capa-

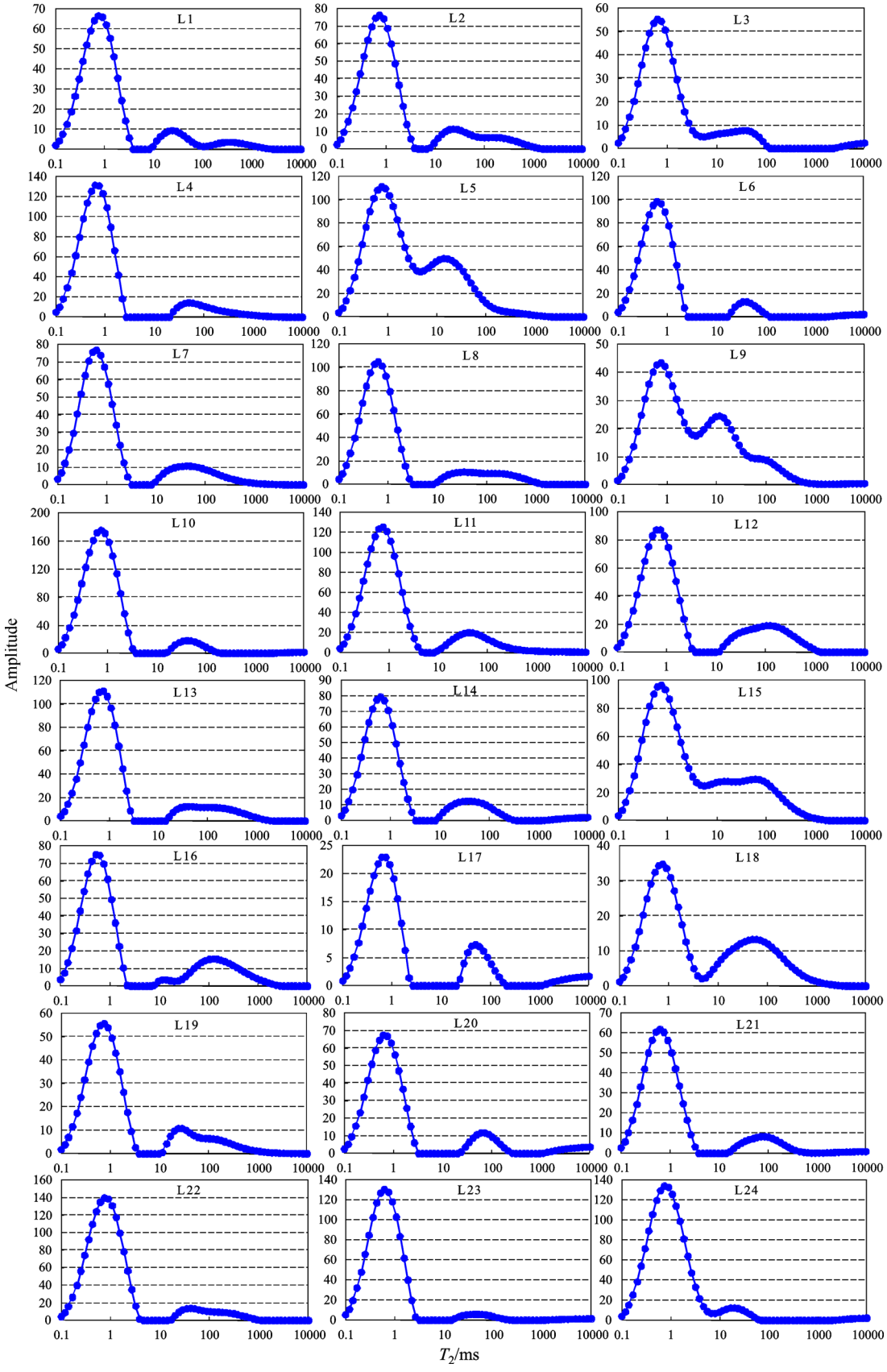

Fig. 7 NMR T_2 relaxation time spectrum of 24 coal core samples.

Table 4 CH_4 isothermal adsorption analyses of 24 coal core samples

Sample	CH_4 isothermal adsorption analysis				
	V_L[a)]/($m^3 \cdot t^{-1}$)			P_L[b)]/Mpa	Correlation coefficient
	V_{Lad}[c)]	V_{Ldaf}[d)]	V_{Lem}[e)]	P_{Lad}[f)]/P_{Ldaf}[g)]/P_{Lem}[h)]	
L1	32.01	47	30	2.45	0.9998
L2	25.81	35.28	24.95	2.24	0.9994
L3	27.44	35.16	25.83	2.27	0.9991
L4	23.97	36.9	22.53	2.52	0.9997
L5	30.65	44.07	28.61	3.13	0.9991
L6	21.71	31.42	20.73	2.04	1
L7	29.04	36.32	28.04	2.07	0.9997
L8	29.87	35.49	28.96	2.06	0.9999
L9	28.59	43.11	27.13	2.81	0.9966
L10	22.82	34.48	21.2	1.97	0.9999
L11	26.12	37.22	24.43	2.11	1
L12	28.83	35.58	26.82	2.06	1
L13	33.63	42.22	32.37	2.52	0.9988
L14	28.33	38.83	26.94	2.24	0.9997
L15	26.23	34.99	24.66	2	0.9999
L16	30.26	39.69	28.86	2.58	0.9992
L17	22.62	31.89	21.43	2.57	0.9986
L18	32.06	36.2	30.47	1.79	0.9999
L19	26.3	38.9	25.12	2.45	0.9981
L20	28.75	35.62	27.82	2.08	0.9999
L21	23.55	42.05	22.47	2.24	0.9995
L22	27.56	39.28	25.73	2.62	1
L23	25.13	40.84	23.94	2.67	1
L24	25.53	39.58	24.06	2.91	0.9997

a) V_L: Langmuir volume; b) P_L: Langmuir pressure; c) and f) V_{Lad} and P_{Lad} : Langmuir volume and pressure (air dry basis); d) and g) V_{Ldaf} and P_{Ldaf} : Langmuir volume and pressure (dry ash-free basis); e) and h) V_{Lem} and P_{Lem} : Langmuir volume and pressure (equilibrium moisture basis).

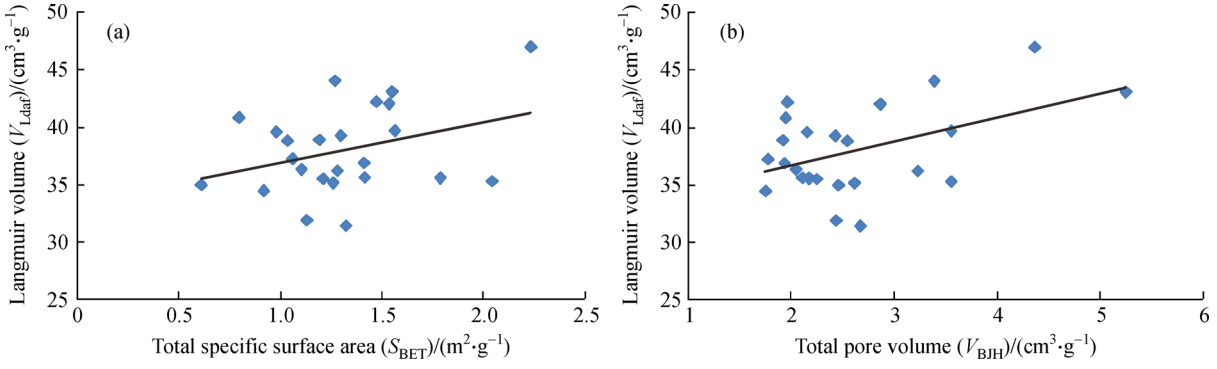

Fig. 8 (a) The relationship between CH_4 adsorption capacity and S_{BET}; (b) The relationship between CH_4 adsorption capacity and V_{BJH}. S_{BET} = the total specific surface area calculated using the BET equation; V_{BJH} = the pore volume calculated using the BJH model; V_{Ldaf} = Langmuir volume (dry ash-free basis).

city, pore surface area, and pore volume.

Pore specific surface area (from BJH model) of super micropores, micropores, mesopores, and macropores of the 24 samples are shown in Table 2. The super micropores specific surface area ($S_{s\text{-}mic}$) ranges from 0.221 to 1.026 m^2/g, with an average of 0.677 m^2/g. The micropores

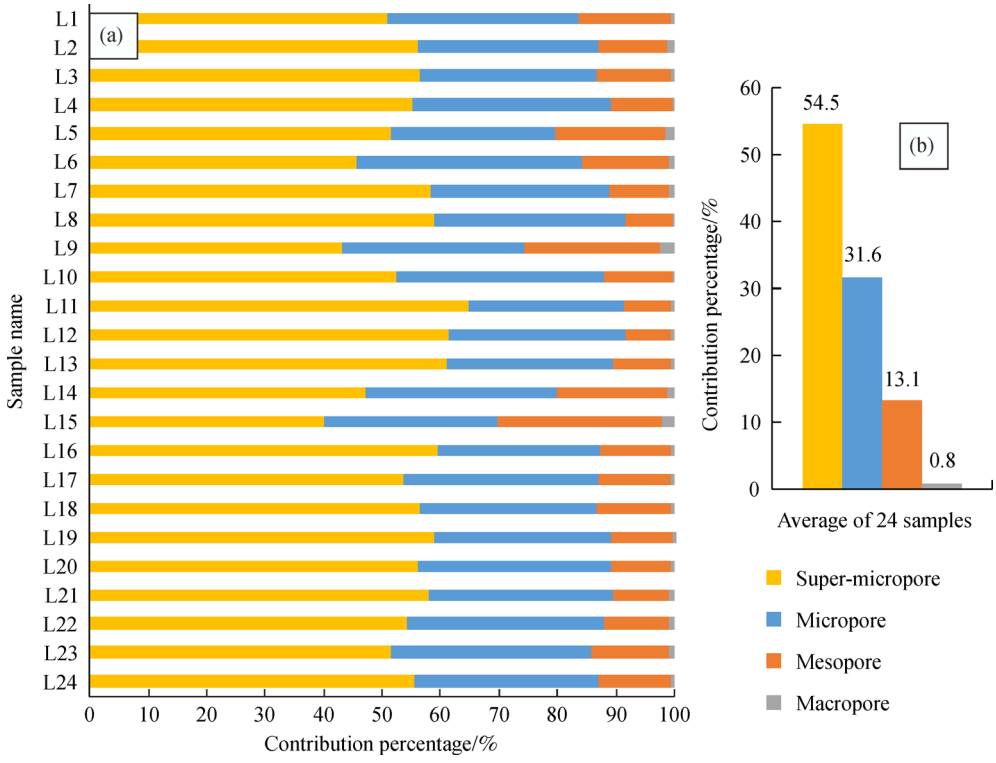

Fig. 9 Pore specific surface area contribution of super micropores, micropores, mesopores, and macropores of 24 coal core samples. (a) Histogram of pore specific surface area contribution percentage of super micropores, micropores, mesopores, and macropores of 24 coal core samples; (b) histogram of the average pore specific surface area contribution percentage of super micropores, micropores, mesopores, and macropores of 24 coal core samples.

specific surface area (S_{mic}) is 0.163−0.663 m^2/g, averaged at 0.389 m^2/g. The mesopores specific surface area (S_{mes}) ranges from 0.084 to 0.363 m^2/g, with an average of 0.159 m^2/g. The macropores specific surface area (S_{mac}) averages 0.010 m^2/g (from 0.002 to 0.036 m^2/g). The contribution of these four types of pores to the total specific surface area can be seen in Table 2 and Fig. 9. Pore volumes (from BJH model) of super micropores, micropores, mesopores, and macropores of the 24 samples are shown in Table 2. The super micropores volume ($V_{s\text{-}mic}$) ranges from 0.171×10^{-3} to 0.773×10^{-3} cm^3/g, with an average of 0.504×10^{-3} cm^3/g. The micropores volume (V_{mic}) ranges from 0.272×10^{-3} to 1.068×10^{-3} cm^3/g, averaged at 0.616×10^{-3} cm^3/g. The mesopores volume (V_{mes}) ranges from 0.577×10^{-3} to 2.739×10^{-3} cm^3/g, with an average of 1.136×10^{-3} cm^3/g. Macropores volume (V_{mac}) ranges from 0.059×10^{-3} to 1.225×10^{-3} cm^3/g, with an average of 0.385×10^{-3} cm^3/g. The contribution of all nano-pores to the total pores volume can be seen in Table 2 and Fig. 10.

In summary, super micropores make the greatest average contribution to the total pore specific surface area, followed by micropores, together they account for 86.1 percent. Mesopores and macropores contribute very little to the total pore specific surface area (Fig. 9). In addition, mesopores give the greatest average contribution to the total pore volume, reaching 42.0%. The pores volume of super micropores and micropores themselves is much smaller than that of mesopores, however, they still contribute 44.1% of the total pores volume. The average contribution of macropores to the total pores volume is much smaller than that of the other three pore types, only 13.9% of all the contribution (Fig. 10). The results indicate that super micropores, micropores, and mesopores make up the bulk of coal porosity, providing extremely large adsorption space with large internal surface area. We can come to a preliminary conclusion that the threshold of pores diameter between adsorption pores and seepage-pores is 100 nm in the studied coals.

4.3 Effects of pore shapes on CH_4 adsorption capacity

From the results in 3.2, we have learned that pore shapes fall into three types (Type A, Type B, and Type C). L3, L6, L7, L8, L17, L18, L19, L21, L23, and L24 samples are mainly composed of both Type A and Type B pores; L10, L11, L12, L13, L14, L15, L16, and L22 samples are mainly composed of Type B pores; L1, L2, L4, L5, L9, and L20 are composed of both Type B and Type C pores. To correlate CH_4 adsorption capacity with nanoscale coal pore shapes, the Langmuir volume data for dry ash-free basis is used. From the V_{Ldaf} results in Table 4, the calculated average V_{Ldaf} of L3, L6, L7, L8, L17, L18, L19, L21, L23,

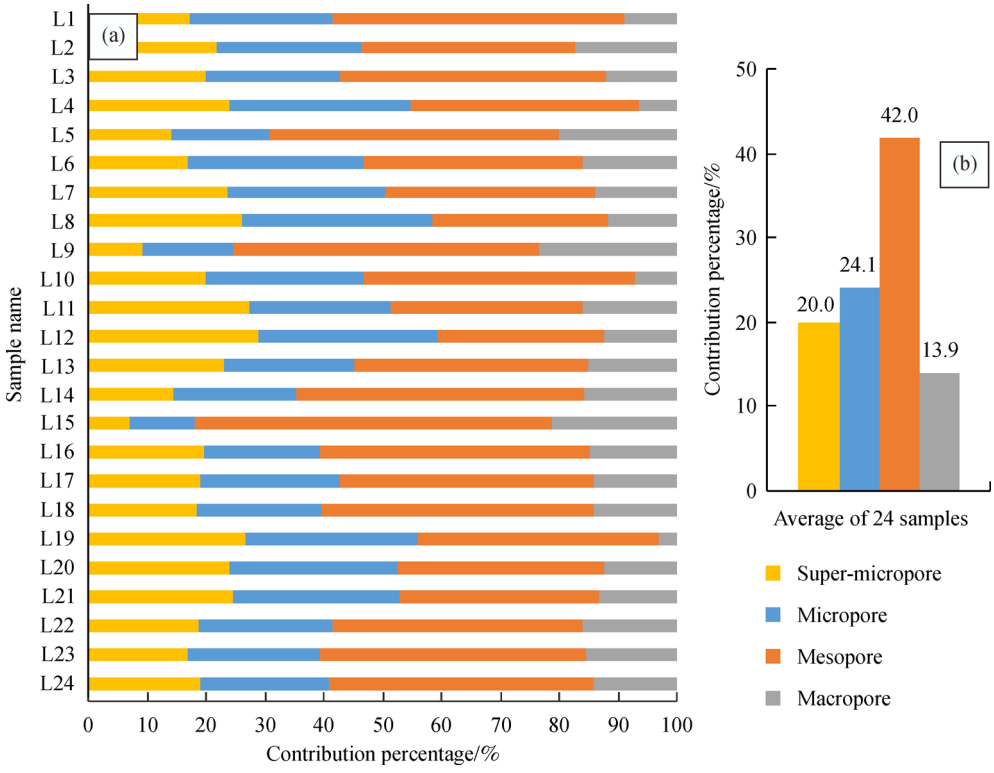

Fig. 10 Pore volume contribution of super micropores, micropores, mesopores, and macropores of 24 coal core samples. (a) Histogram of pore volume contribution percentage of super micropores, micropores, mesopores, and macropores of 24 coal core samples; (b) histogram of the average pore volume contribution percentage of super micropores, micropores, mesopores, and macropores of 24 coal core samples.

and L24 samples is 36.75 cm^3/g; the average V_{Ldaf} of L1, L2, L4, L5, L9, and L20 is 40.33 cm^3/g; and the average V_{Ldaf} of L10, L11, L12, L13, L14, L15, L16, and L22 is 37.79 cm^3/g. So there seems to be a significant trend of the V_{Ldaf}: Type B + Type C > Type B > Type A + Type B, corresponding to the prediction that "ink bottle" pores have the largest CH_4 adsorption capacity, followed by semi-opened pores, with the opened pores possessing the least CH_4 adsorption capacity. We can further predict that anthracite pores with more irregular shapes have higher CH_4 adsorption capacity.

4.4 Effects of NMR physical properties on CH_4 adsorption capacity

From the experimental data of NMR analyses (Table 3) and Langmuir volume calculated on a dry ash-free basis (Table 4), the relationships among CH_4 adsorption capacity, NMR porosity, NMR permeability, and the bound water saturation are discussed.

A plot of V_{Ldaf} with respect to NMR porosity is given in Fig. 11(a), showing that a positive correlation exists between CH_4 adsorption capacity and NMR porosity, as demonstrated by the increase in CH_4 adsorption capacity with the increase in NMR porosity. It is generally known that porosity is the ratio of the total pore space to the total sample volume, so there is also a positive relationship between the total pore space. That is, the positive correlation between CH_4 adsorption capacity and NMR porosity can prove that anthracite pores are mainly composed of adsorption pores (super-micropore, micropores, and mesopores).

Figure 11(b) shows the relationship between V_{Ldaf} and NMR permeability. A positive correlation occurs when NMR permeability is less than approximately 8×10^{-3} md, but a negative correlation occurs when it is greater than 8×10^{-3} md. This behavior is caused by macropores (seepage-pores), which are mainly permeable pathways for gas and water migration (Yao et al., 2009). When coal NMR permeability is less than 8×10^{-3} md, pores contain very few macropores, and mesopores play the major role in increasing coal permeability. The increase in NMR permeability means that the number of mesopores gradually increases, leading to the increase in CH_4 adsorption capacity, because mesopores are one type of adsorption pores. When coal NMR permeability is larger than 8×10^{-3} md, it can be predicted that some macropores in coal start to provide pathways for fluid migration, the number of macropores increases with the increasing NMR permeability; in other words, the number of adsorption pores becomes a relative reduction, so the CH_4 adsorption capacity decreases with the increase of NMR permeability.

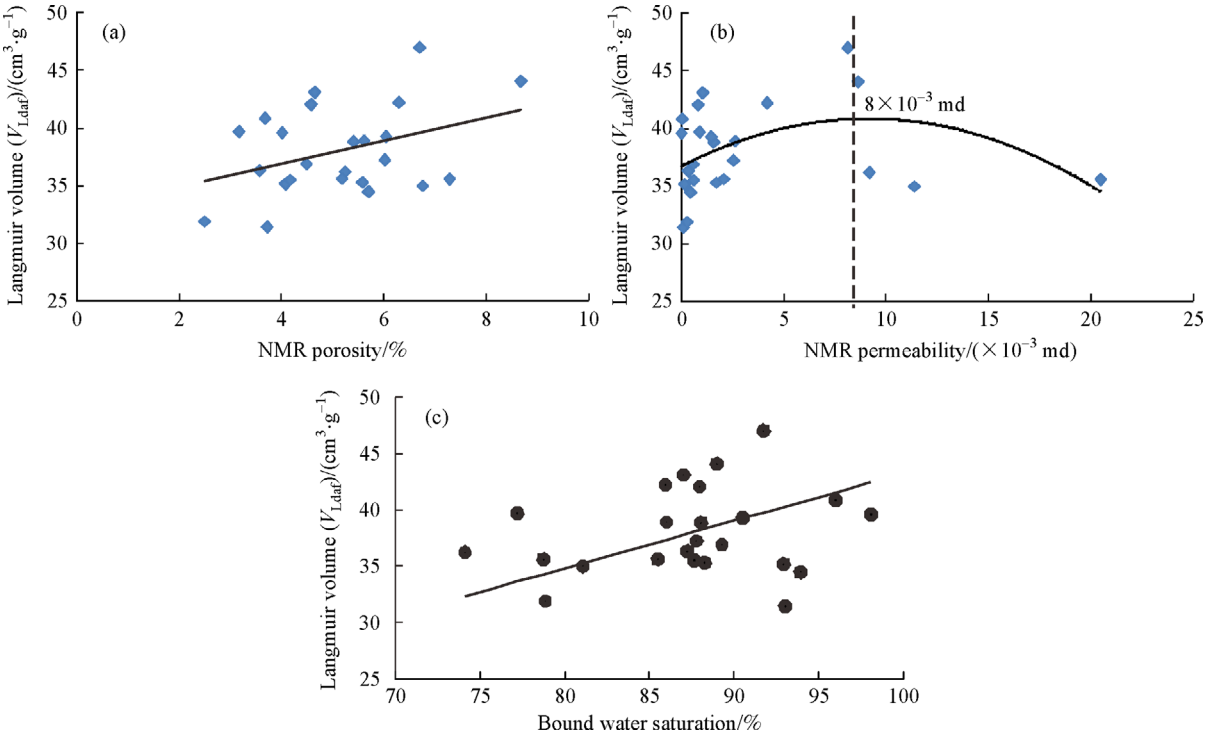

Fig. 11 (a) The relationship between CH_4 adsorption capacity and NMR porosity; (b) The relationship between CH_4 adsorption capacity and NMR permeability; (c) The relationship between CH_4 adsorption capacity and the bound water saturation. V_{Ldaf} = Langmuir volume (dry ash-free basis).

The relationship between V_{Ldaf} and the bound water saturation is shown in Fig. 11(c). We can see that there is a positive correlation between CH_4 adsorption capacity and the bound water saturation. That is, CH_4 adsorption capacity increases with the increase in the bound water saturation. This is because pores internal surface-adsorbed water molecules of coals increase with the increase in the bound water saturation, thus providing CH_4 with more adsorption sites.

5 Conclusions

In this paper, a combined experiment (e.g., coal maceral analysis, vitrinite reflectance tests, proximate analysis, ultimate analysis, low-temperature N_2 adsorption-desorption experiments, NMR analysis, and CH_4 isothermal adsorption experiments) were conducted on 24 anthracite samples to determine the effects of pore surface, pore volume, pore size ranges, pore shapes, and physical properties on CH_4 adsorption capacity. Anthracites with higher pore surface area and volume have higher CH_4 adsorption capacities due to the availability of more sites and space for CH_4 adsorption. Nano-pores are divided into super micropores (<4 nm), micropores (4–10 nm), mesopores (10–100 nm), and macropores (>100 nm). Super micropores are the largest category of pores, but mesopores and macropores make more contribution to the total pore volume. Super micropores, micropores, and mesopores make up the bulk of coal porosity, providing extremely large adsorption space with large internal surface area, which leads to the prediction that the threshold of pores diameter between adsorption pores and seepage-pores is 100 nm in the studied anthracites. Coal pores are divided into three types based on pore shape, namely opened pores, semi-closed pores, and "ink bottle" pores. The "ink bottle" pores have the largest CH_4 adsorption capacity, followed by semi-opened pores, and then the opened pores. Therefore, anthracite pores with more irregular shapes have higher CH_4 adsorption capacity. CH_4 adsorption capacity increased with the increase in NMR porosity and the bound water saturation, respectively. CH_4 adsorption capacity is positively correlated with NMR permeability when NMR permeability is less than 8×10^{-3} md, and negatively correlated when the permeability is greater than 8×10^{-3} md.

Acknowledgements This research was funded by the Open Foundation of Key Laboratory of Tectonics and Petroleum Resources (China University of Geosciences) (No. TPR-2016-04), the Open Foundation of Shandong Provincial Key Laboratory of Depositional Mineralization & Sedimentary Mineral, (Shandong University of Science and Technology) (No. DMSM2017031), the Youth Science and Technology Innovation Fund Project (Xi'an Shiyou University) (No. 290088259), the National Science and Technology Major Project (No. 2017ZX05039001-002), the National Natural

Science Foundation of China (Grant Nos. 41702127 and 41772150), the Scientific Research Program Funded by Shaanxi Provincial Education Department (No. 17JK0617).

References

Ayers W B Jr (2002). Coalbed gas systems, resources, and production and a review of contrasting cases from the San Juan and Powder River basins. AAPG Bull, 86(11): 1853–1890

Barrett E P, Joyner L G, Halenda P P (1951). The determination of pore volume and area distributions in porous substances. I. Computations from nitrogen isotherms. J Am Chem Soc, 73(1): 373–380

Brunauer S, Emmett P H, Teller E (1938). Adsorption of gases in multimolecular layers. J Am Chem Soc, 60(2): 309–319

Cai Y D, Liu D M, Pan Z J, Yao Y B, Li J Q, Qiu Y K (2013). Pore structure and its impact on CH_4 adsorption capacity and flow capability of bituminous and subbituminous coals from Northeast China. Fuel, 103: 258–268

Chen P, Tang X Y (2001). The research on the adsorption of nitrogen in low-temperature and micro-pore properties in coal. Journal of China Coal Society, 26: 552–556 (in Chinese)

Coates G R, Xiao L Z, Prammer M G (1999). NMR Logging Principles and Applications. Houston: Gulf Publishing Company

Cuerda-Correa E M, Díaz-Díez M A, Macías-García A, Gañán-Gómez J (2006). Determination of the fractal dimension of activated carbons: two alternative methods. Appl Surf Sci, 252(17): 6102–6105

De Boer J H (1958). The shape of capillaries. In: Everett D H, Stone F S, eds. The Structure and Properties of Porous Materials. London: Butterworth, 25–195

Diduszko R, Swiatkowski A, Trznadel B J (2000). On surface of micropores and fractal dimension of activated carbon determined on the basis of adsorption and SAXS investigations. Carbon, 38(8): 1153–1162

Faulon J L, Mathews J P, Carlson G A, Hatcher P G (1994). Correlation between microporosity and fractal dimension of bituminous coal based on computer- generated models. Energy Fuels, 8(2): 408–414

Fu X, Qin Y, Xue X (2000). Application of fractal theory on physical properties in coal reservoirs. Coal, 9(4): 1–3 (in Chinese)

Gan H, Nandi S P, Walker P L Jr (1972). Nature of porosity in American coals. Fuel, 51(4): 272–277

Giffin S, Littke R, Klaver J, Urai J L (2013). Application of BIB–SEM technology to characterize macropore morphology in coal. Int J Coal Geol, 114(4): 85–95

Gray I (1987). Reservoir engineering in coal seams: part 1—The physical process of gas storage and movement in coal seams. SPE (Society of Petroleum Engineers) Reservoir Evaluation & Engineering, 2(1): 28–34

Gürdal G, Yalçın M (2001). Pore volume and surface area of the Carboniferous coals from the Zonguldak basin (NW Turkey) and their variations with rank and maceral composition. Int J Coal Geol, 48(1–2): 133–144

Hao Q (1987). On morphological character and origin of micropores in coal. Journal of China Coal Society, 4: 51–54 (in Chinese)

Hodgkins M A, Howard J J (1999). Application of NMR logging to reservoir characterization of low-resistivity sands in the Gulf of Mexico. AAPG Bull, 83(1): 114–127

Hodot B B (1966). Outburst of Coal and Coalbed Gas (Chinese Translation). Beijing: China Industry Press

ICS (International Commission on Stratigraphy) (2017). International Chronostratigraphic Chart (v 2017/02)

Karacan C O, Okandan E (2001). Adsorption and gas transport in coal microstructure: investigation and evaluation by quantitative X-ray CT imaging. Fuel, 80(4): 509–520

Kenyon W E (1992). Nuclear magnetic resonance as a petrophysical measurement. International Journal of Radiation Applications and Instrumentation. Part E. Nuclear Geophysics, 6: 153–171

Mahamud M, López Ó, Pis J J, Pajares J A (2004). Textural characterization of chars using fractal analysis. Fuel Process Technol, 86(2): 135–149

Mahnke M, Mögel H J (2003). Fractal analysis of physical adsorption on material surfaces. Colloids Surf A Physicochem Eng Asp, 216(1−3): 215–228

Mitropoulos A C, Stefanopoulos K L, Kanellopoulos N K (1998). Coal studies by small angle X-ray scattering. Microporous Mesoporous Mater, 24(1−3): 29–39

Nakagawa T, Komaki I, Sakawa M, Nishikawa K (2000). Small angle X-ray scattering study on change of fractal property of Witbank coal with heat treatment. Fuel, 79(11): 1341–1346

Pan J N, Lv M M, Bai H L, Hou Q L, Li M, Wang Z Z (2017). Effects of metamorphism and deformation on the coal macromolecular structure by laser raman spectroscopy. Energy Fuels, 31(2): 1136–1146

Pan J N, Niu Q H, Wang K, Shi X H, Li M (2016). The closed pores of tectonically deformed coal studied by small-angle X-ray scattering and liquid nitrogen adsorption. Microporous Mesoporous Mater, 224: 245–252

Pan J N, Zhao Y Q, Hou Q L, Jin Y (2015a). Nanoscale pores in coal related to coal rank and deformation structures. Transp Porous Media, 107(2): 543–554

Pan J N, Zhu H T, Hou Q L, Wang H C, Wang S (2015b). Macromolecular and pore structures of Chinese tectonically deformed coal studied by atomic force microscopy. Fuel, 139: 94–101

Radlinski A P, Mastalerz M, Hinde A L, Hainbuchner M, Rauch H, Baron M, Lin J S, Fan L, Thiyagarajan P (2004). Application of SAXS and SANS in evaluation of porosity, pore size distribution and surface area of coal. Int J Coal Geol, 59(3−4): 245–271

Radovic L R, Menon V C, LeonY , Leon C A, Kyotani T, Danner R P, Anderson S, Hatcher P G (1997). On the porous structure of coals: evidence for an interconnected but constricted micropore system and implications for coalbed methane recovery. Adsorption, 3(3): 221–232

Rigby S P (2005). Predicting surface diffusivities of molecules from equilibrium adsorption isotherms. Colloids Surf A Physicochem Eng Asp, 262(1−3): 139–149

Sastry P U, Sen D, Mazumder S, Chandrasekaran K S (2000). Structural variations in lignite coal: a small angle X-ray scattering investigation. Solid State Commun, 114(6): 329–333

Shan C A, Zhang T S, Guo J J, Zhang Z, Yang Y (2015). Characterization of the micropore systems in high-rank coal reservoirs of the southern Sichuan Basin, China. AAPG Bull, 99

(11): 2099–2119

Shi J Q, Durucan S (2005). Gas storage and flow in coalbed reservoirs: implementation of a bidisperse pore model for gas diffusion in a coal matrix. SPE Reservoir Eval Eng, 8(02): 169–175

Sing K S W (1982). Reporting physisorption data for gas/solid systems with special reference to the determination of surface area and porosity. Pure Appl Chem, 54(4): 2201–2218

Yao Y B, Liu D M (2006). Pore system characteristics of coal reservoirs and their influence on recovering of coalbed methane in Henan coalfields. Coal Science and Technology, 34: 64–68 (in Chinese)

Yao Y B, Liu D M, Huang W H, Tang D Z, Tang S H (2006). Research on the pore-fractures system properties of coalbed methane reservoirs and recovery in Huainan and Huaibei coal-fields. Journal of China Coal Society, 3: 163–168 (in Chinese)

Yao Y B, Liu D M, Tang D Z, Tang S H, Huang W H (2008). Fractal characterization of adsorption pores of coals from North China: an investigation on the CH_4 adsorption capacity of coal. Int J Coal Geol, 73(1): 27–42

Yao Y B, Liu D M, Tang D Z, Tang S H, Huang W H, Liu Z H, Che Y (2009). Fractal characterization of seepage-pores of coals from China: an investigation on permeability of coals. Comput Geosci, 35 (6): 1159–1166